

Quasi-Monochromatic Flash X-Ray Generator Utilizing Disk-Cathode Molybdenum Tube

Eiichi SATO, Michiaki SAGAE, Etsuro TANAKA¹, Yasuomi HAYASI, Rudolf GERMER², Hidezo MORI³, Toshiaki KAWAI⁴, Toshio ICHIMARU⁵, Shigehiro SATO⁶, Kazuyoshi TAKAYAMA⁷ and Hideaki IDO⁸

Department of Physics, Iwate Medical University, 3-16-1 Honchodori, Morioka 020-0015, Japan

¹Department of Nutritional Science, Faculty of Applied Bio-science, Tokyo University of Agriculture, 1-1-1 Sakuragaoka, Setagaya-ku 156-8502, Japan

²ITP, FHTW FB1 and TU-Berlin, Blankenhainer Str. 9, D 12249 Berlin, Germany

³Department of Cardiac Physiology, National Cardiovascular Center Research Institute, 5-7-1 Fujishiro-dai, Suita, Osaka 565-8565, Japan

⁴Electron Tube Division #2, Hamamatsu Photonics Inc., 314-5 Shimokanzo, Toyooka Village, Iwata-gun 438-0193, Japan

⁵Department of Radiological Technology, School of Health Sciences, Hirosaki University, 66-1 Honcho, Hirosaki 036-8564, Japan

⁶Department of Microbiology, School of Medicine, Iwate Medical University, 19-1 Uchimaru, Morioka 020-8505, Japan

⁷Shock Wave Research Center, Institute of Fluid Science, Tohoku University, 2-1-1 Katahira, Aoba-ku, Sendai 980-8577, Japan

⁸Department of Applied Physics and Informatics, Faculty of Engineering, Tohoku Gakuin University, 1-13-1 Chuo, Tagajo 985-8537, Japan

(Received April 2, 2004; accepted June 14, 2004; published October 8, 2004)

High-voltage condensers in a polarity-inversion two-stage Marx surge generator are charged from -40 to -60 kV using a power supply, and the electric charges in the condensers are discharged to an X-ray tube after closing the gap switches in the surge generator using a trigger device. The X-ray tube is a demountable diode, and the turbomolecular pump evacuates air from the tube with a pressure of approximately 1 mPa. Sharp K-series characteristic X-rays of molybdenum are produced without using a monochromatic filter, since the tube utilizes a disk cathode and a rod target, and bremsstrahlung rays are not emitted in the opposite direction to that of electron acceleration. The peak tube voltage increased with increasing charging voltage and increasing space between the target and cathode electrodes. At a charging voltage of -60 kV and a target-cathode space of 1.0 mm, the peak tube voltage and current were 110 kV and 0.75 kA, respectively. The pulse width ranged from 40 to 100 ns, and the maximum dimension of the X-ray source was 3.0 mm in diameter. The number of generator-produced K photons was approximately 7×10^{14} photons/cm²·s at 0.5 m from the source. [DOI: 10.1143/JJAP.43.7324]

KEYWORDS: flash X-ray, characteristic X-ray, quasi-monochromatic radiography, bremsstrahlung X-ray distribution

1. Introduction

Flash X-ray generators have been developed as a powerful tool in high-speed radiography because they produce extremely short X-ray pulses of less than 1 μ s. Currently, most generators utilize a multistage Marx surge generator^{1,2)} in order to produce high-photon-energy flash X-rays by increasing the maximum tube voltage. On the other hand, soft flash X-ray generators³⁻⁷⁾ with photon energies of less than 150 keV can be applied to biomedicine, and the repetition rate has been increased to the sub-kilohertz order.⁸⁾

High-dose-rate monochromatic X-rays are produced by a synchrotron in conjunction with single crystals and have been applied to X-ray phase imaging^{9,10)} and microangiography.¹¹⁾ Subsequently, because extremely high-dose-rate quasi-monochromatic X-rays are produced from the axial direction of weakly ionized linear plasma,¹²⁻¹⁴⁾ high-speed biomedical radiography has been performed. However, the bremsstrahlung X-rays are produced using targets of molybdenum, silver, cerium, and tungsten, since high-photon-energy bremsstrahlung X-rays are not absorbed effectively in the linear plasma. In addition, in cases where cold cathode triodes are employed, it is difficult to increase the condenser charging voltage to increase the photon energies of characteristic X-rays due to vacuum breakdown; the target voltage is equal to the charging voltage.

Because bremsstrahlung X-ray intensity varies with changes in the angle and direction of electron acceleration, characteristic X-rays are produced without using a monochromatic filter by selecting the irradiation direction. Although bremsstrahlung intensity is proportional to the atomic number, the angle selection will be a useful technique to produce quasi-monochromatic X-rays.

In this article, we describe a compact flash X-ray

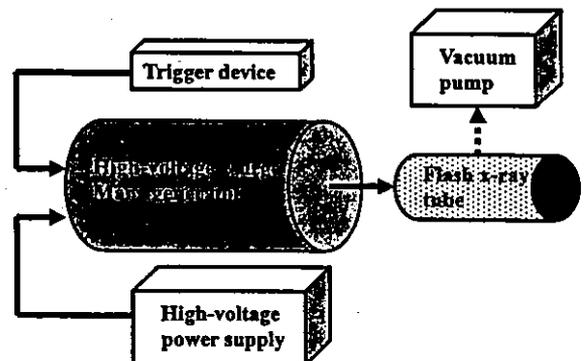


Fig. 1. Block diagram of compact quasi-monochromatic flash X-ray generator.

generator utilizing a molybdenum-target radiation tube, used to perform a preliminary experiment for generating quasi-monochromatic X-rays using the angle dependence of bremsstrahlung rays.

2. Generator

2.1 High-voltage circuit

Figure 1 shows a block diagram of a compact quasi-monochromatic flash X-ray generator. This generator consists of the following components: a constant high-voltage power supply, a polarity-inversion two-stage surge Marx generator with a capacity during main discharge of 425 pF, a trigger device for the surge generator, a turbomolecular pump, and a flash X-ray tube. Since the electric circuit of the surge generator employs a polarity-inversion two-stage Marx line (Fig. 2), the surge produces twice the potential of the condenser charging voltage. When two condensers inside of the surge generator are charged from -40 to

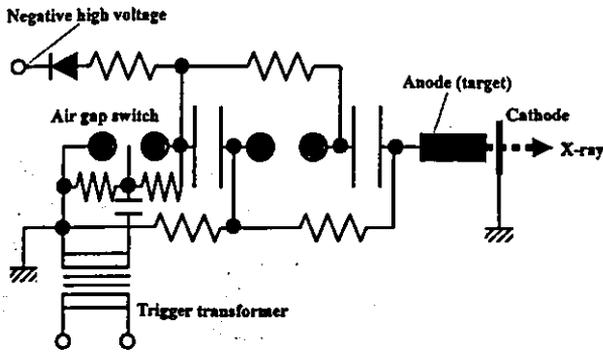


Fig. 2. Circuit diagram of flash X-ray generator.

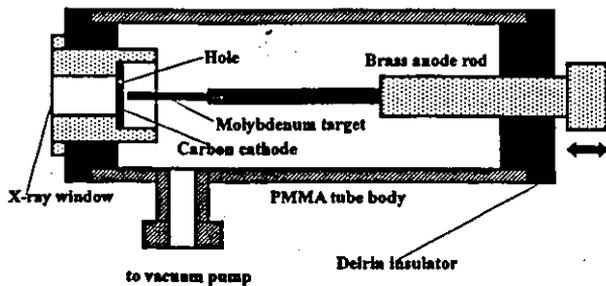


Fig. 3. Schematic drawing of flash X-ray tube.

-60 kV, the ideal output voltage ranges from 80 to 120 kV.

2.2 X-ray tube

The X-ray tube is of the demountable diode type, as illustrated in Fig. 3. This tube is connected to the turbomolecular pump with a pressure of approximately 1 mPa and consists of the following major devices: a rod-shaped molybdenum target, a disk cathode made of graphite, a polyethylene terephthalate (Mylar) X-ray window 0.25 mm in thickness, and a polymethyl methacrylate (PMMA) tube body. The target-cathode (T-C) space was regulated from the outside of the X-ray tube by rotating the anode rod, and

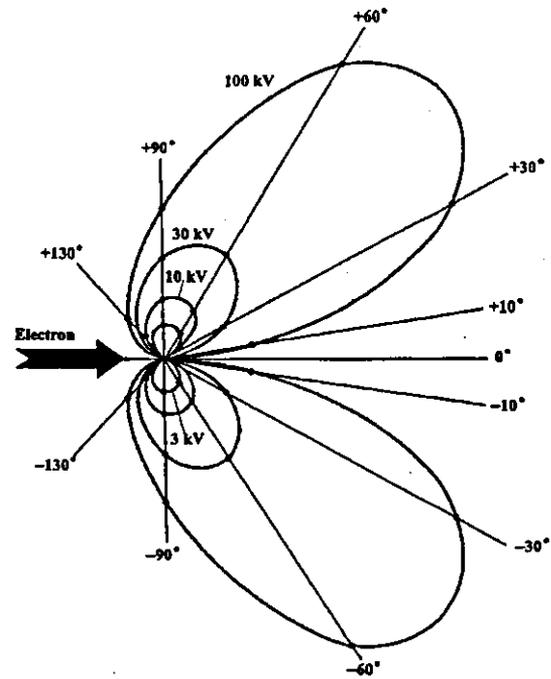


Fig. 4. Bremsstrahlung X-ray intensity distribution vs angle.

the transmission X-rays are obtained through a 1.0 mm-thick graphite cathode and an X-ray window. Because bremsstrahlung rays are not emitted in the opposite direction to that of electron acceleration (Fig. 4), characteristic X-rays can be produced.

3. Characteristics

3.1 Tube voltage and current

Tube voltage and current were measured using a high-voltage divider with an input impedance of 10 kΩ and a current transformer, respectively (Figs. 5 and 6). The voltage and current roughly displayed damped oscillations. At a constant T-C space of 1.0 mm, peak voltage increased slightly with increasing charging voltage. In contrast, peak

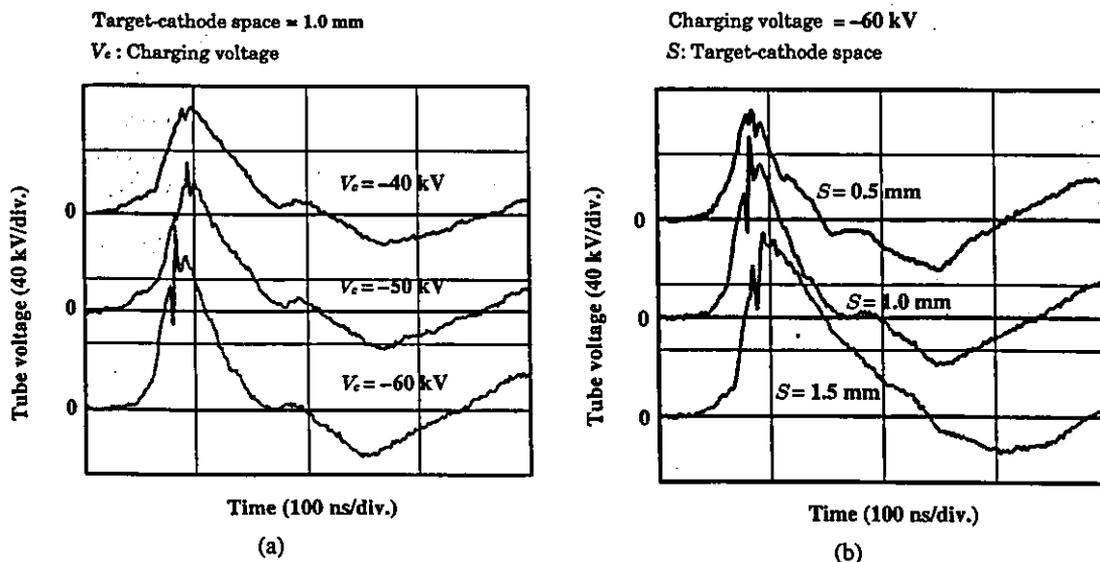


Fig. 5. Variations in tube voltage with changes in (a) charging voltage and (b) space.

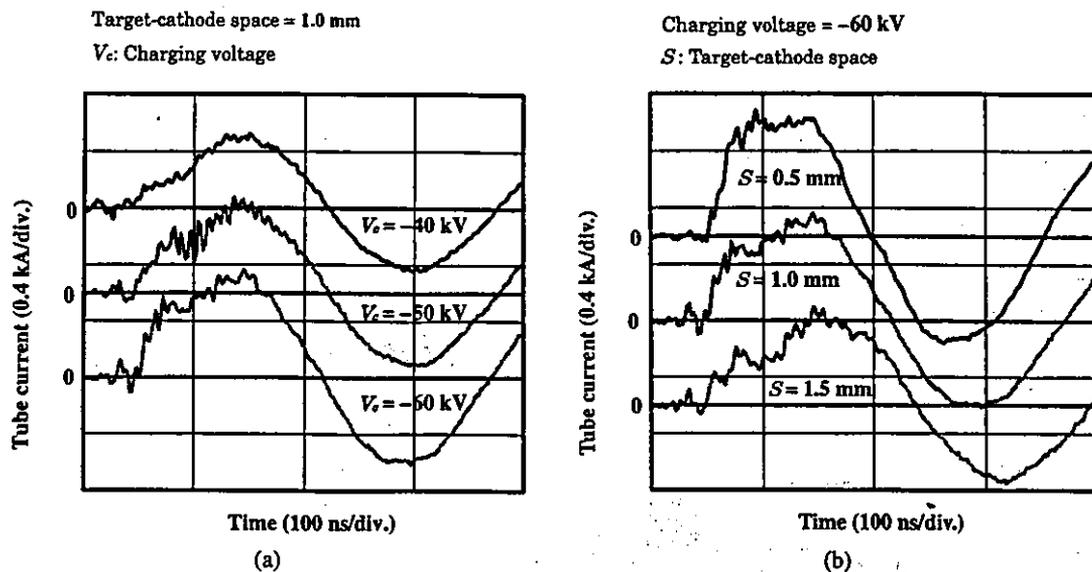


Fig. 6. Tube currents with changes in (a) charging voltage and (b) space.

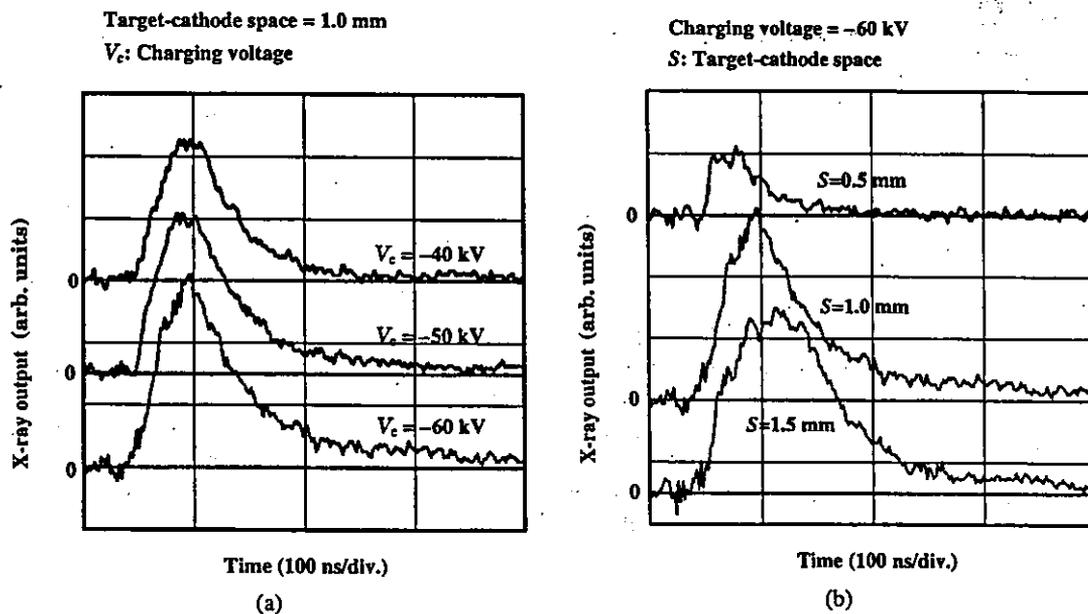


Fig. 7. X-ray outputs according to changes in (a) charging voltage and (b) space.

voltage substantially increased when T-C space was increased at a constant charging voltage of -60 kV. Subsequently, peak tube current increased with increasing charging voltage. When T-C space was increased, current rise time increased, and peak current decreased. At a charging voltage of -60 kV and a T-C space of 1.0 mm, peak tube voltage and current were 110 kV and 0.75 kA, respectively.

3.2 X-ray output

X-ray output pulse was detected using a combination of a plastic scintillator and a photomultiplier (Fig. 7). When the charging voltage was increased, the pulse height increased, but the width seldom varied. Next, with increases in the T-C space, the height was maximized, and the width increased. In the present work, the width ranged from 40 to 100 ns. Next,

the time-integrated X-ray intensity measured using a thermoluminescence dosimeter (Kyokko TLD Reader 1500 having MSO-S elements without energy compensation) was approximately $3.0 \mu\text{C}/\text{kg}$ at 0.5 m from the X-ray source with a charging voltage of -60 kV and a T-C space of 1.0 mm.

3.3 X-ray source

In order to measure the images of the X-ray source, we employed a pinhole camera with a hole diameter of $100 \mu\text{m}$ (Fig. 8). When the charging voltage was increased, the plasma X-ray source grew, and both spot dimension and intensity increased. The maximum dimension was almost equal to the target diameter and had a value of approximately 3.0 mm.

V_c : Charging voltage

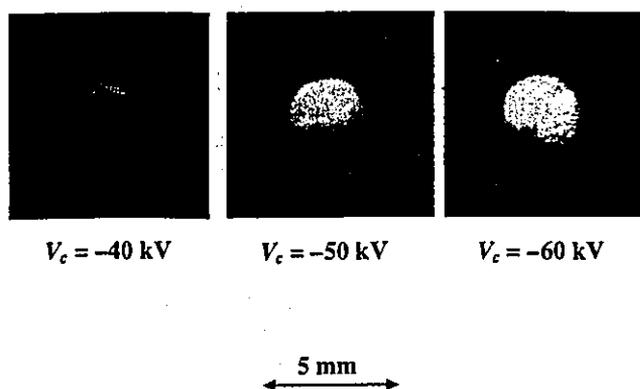


Fig. 8. Images of X-ray source with changes in charging voltage at constant space between target and cathode electrodes.

3.4 X-ray spectra

X-ray spectra were measured by a transmission-type spectrometer with a lithium fluoride curved crystal 0.5 mm in thickness. The spectra were measured using a computed radiography (CR) system¹⁵⁾ (Konica Regius 150) with a wide dynamic range, and relative X-ray intensity was calculated from Dicom digital data. Figure 9 shows the measured spectra from the molybdenum target. We observed sharp lines of K-series characteristic X-rays, while bremsstrahlung rays were hardly detected. The characteristic X-ray intensity of the $K\alpha$ and $K\beta$ lines substantially increased with increasing charging voltage.

4. Radiography

Flash radiography was performed using the CR system at 0.5 m from the X-ray source, and the charging voltage and the T-C space were -60 kV and 1.0 mm, respectively.

Firstly, rough measurements of spatial resolution were made using wires. Figure 10 shows radiograms of tungsten wires coiled around a pipe made of polymethyl methacry-

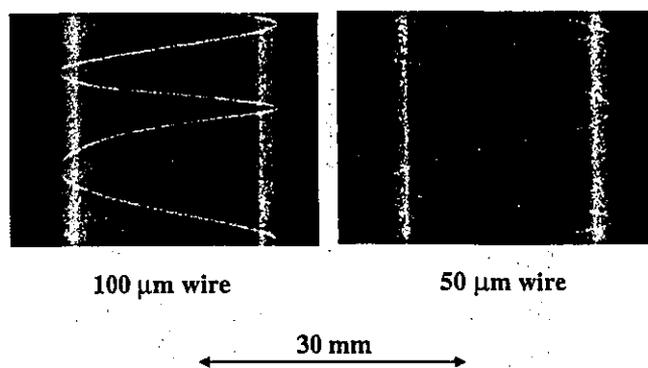


Fig. 10. Radiograms of tungsten wires of 50 and 100 μ m in diameter coiled around pipes made of polymethyl methacrylate.

late. Although the image contrast increased with increasing wire diameter, a 50- μ m-diameter wire could be observed.

An image of plastic bullets falling into a polypropylene beaker from a glass test tube is shown in Fig. 11. Because the X-ray pulse widths were approximately 60 ns, the stop-motion image of bullets could be obtained. Figure 12 shows an angiogram of a rabbit heart; iodine-based microspheres of 15 μ m in diameter were used, and fine blood vessels of approximately 100 μ m were visible.

5. Discussion

Concerning the spectrum measurement, sharp molybdenum K-series characteristic X-rays were obtained, and monochromatic $K\alpha$ lines can be obtained using a zirconium filter. The photon energies of characteristic X-rays are determined by the target element, and the X-ray intensity increases with increasing tube voltage by increasing the charging voltage. As compared with the plasma flash X-ray generator utilizing a molybdenum target triode,¹³⁾ bremsstrahlung X-rays were hardly observed at all even when higher tube voltages were applied to the diode, since the characteristic X-rays were produced from the target tip. Because the maximum tube voltage can be increased easily, and high-photon-energy K-series characteristic X-rays from

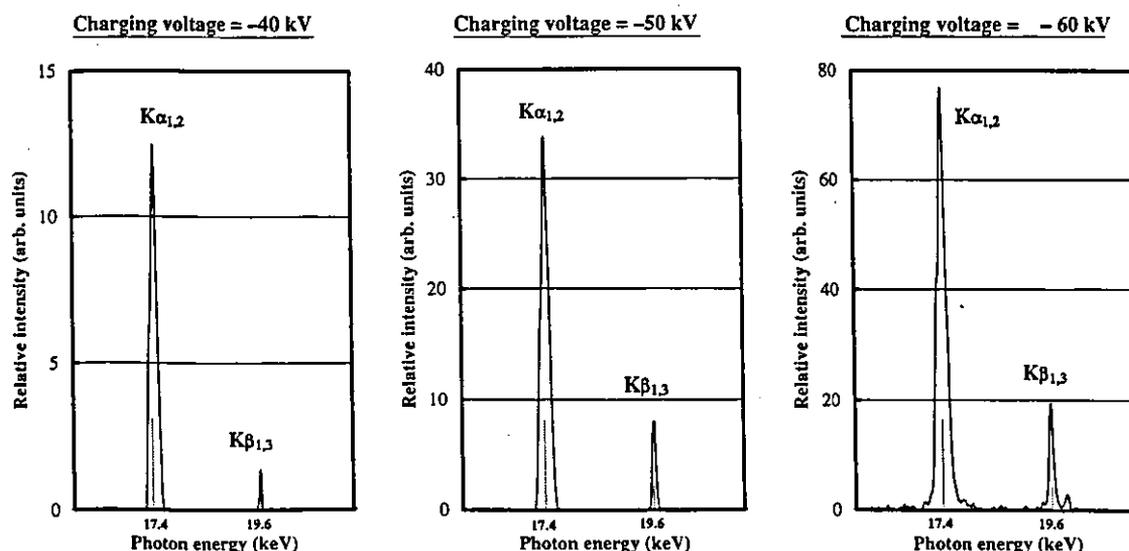
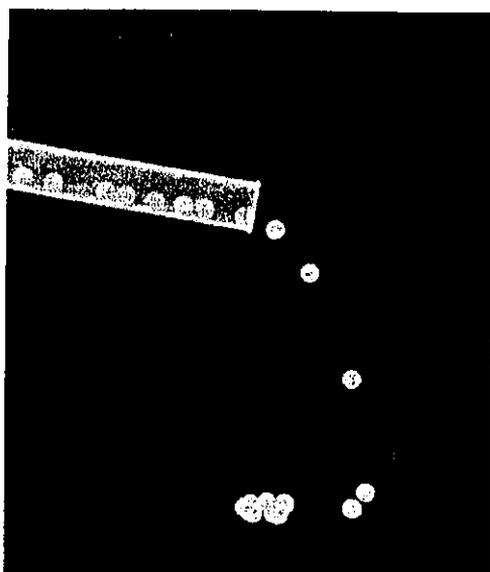


Fig. 9. X-ray spectra from weakly ionized molybdenum plasma according to changes in charging voltage with space of 1.0 mm.



50 mm

Fig. 11. Radiograms of plastic bullets falling into polypropylene beaker from glass test tube.

100 μm tungsten wire



30 mm

Fig. 12. Angiogram of rabbit heart.

the cerium or tungsten target can be produced. In particular, the cerium target is very useful in order to perform microangiography using iodine-based contrast mediums.

In this research, although the number of generator-produced characteristic K photons was approximately 7×10^{14} photons/cm²·s at 0.5 m from the source, the number can be increased easily by increasing the electrostatic energy in the condensers.

Using this generator, because the photon energies of characteristic X-rays can be selected, various quasi-monochromatic high-speed radiographies, such as high contrast microangiography and photon-counting radiography for decreasing noise from radiograms, will be possible.

Acknowledgment

This work was supported by Grants-in-Aid for Scientific Research (13470154, 13877114, and 16591222) and Advanced Medical Scientific Research from MECSSST, Grants from Keiryō Research Foundation, JST (Test of Fostering Potential), NEDO, and MHLW (HLSRG, RAMT-nano-001, RHGTEFB-genome-005, and RGCD13C-1).

- 1) A. Mattsson: *Physica Scripta* **5** (1972) 99.
- 2) R. Germer: *J. Phys. E: Sci. Instrum.* **12** (1979) 336.
- 3) E. Sato, H. Isobe and F. Hoshino: *Rev. Sci. Instrum.* **57** (1986) 1399.
- 4) E. Sato, M. Sagae, K. Takahashi, A. Shikoda, T. Oizumi, Y. Hayasi, Y. Tamakawa and T. Yanagisawa: *Med. & Biol. Eng. & Comput.* **32** (1994) 295.
- 5) A. Shikoda, E. Sato, M. Sagae, T. Oizumi, Y. Tamakawa and T. Yanagisawa: *Rev. Sci. Instrum.* **65** (1994) 850.
- 6) E. Sato, M. Sagae, A. Shikoda, K. Takahashi, T. Oizumi, M. Yamamoto, A. Takabe, K. Sakamaki, Y. Hayasi, H. Ojima, K. Takayama and Y. Tamakawa: *Proc. SPIE* **2869** (1996) 937.
- 7) K. Takahashi, E. Sato, M. Sagae, T. Oizumi, Y. Tamakawa and T. Yanagisawa: *Jpn. J. Appl. Phys.* **33** (1994) 4146.
- 8) E. Sato, K. Takahashi, M. Sagae, S. Kimura, T. Oizumi, Y. Hayasi, Y. Tamakawa and T. Yanagisawa: *Med. & Biol. Eng. & Comput.* **32** (1994) 289.
- 9) T. J. Davis, D. Gao, T. E. Gureyev, A. W. Stevenson and S. W. Wilkins: *Nature* **373** (1995) 595.
- 10) A. Momose, T. Takeda, Y. Itai and K. Hirano: *Nature Medicine* **2** (1996) 473.
- 11) H. Mori *et al.*: *Radiology* **201** (1996) 173.
- 12) E. Sato, Y. Hayasi, R. Germer, E. Tanaka, H. Mori, T. Kawai, H. Obara, T. Ichimaru, K. Takayama and H. Ido: *Jpn. J. Med. Imag. Inform. Sci.* **20** (2003) 148.
- 13) E. Sato, Y. Hayasi, R. Germer, E. Tanaka, H. Mori, T. Kawai, H. Obara, T. Ichimaru, K. Takayama and H. Ido: *Jpn. J. Med. Phys.* **23** (2003) 123.
- 14) E. Sato, Y. Hayasi, R. Germer, E. Tanaka, H. Mori, T. Kawai, T. Ichimaru, K. Takayama and Hideaki Ido: *Rev. Sci. Instrum.* **74** (2003) 5236.
- 15) E. Sato, K. Sato and Y. Tamakawa: *Ann. Rep. Iwate Med. Univ. Sch. Lib. Arts and Sci.* **35** (2000) 13.

研究論文

Monochromatic polycapillary imaging utilizing a computed radiography system

Michiaki Sagae^{1)*}, Eiichi Sato¹⁾, Yasuomi Hayasi¹⁾, Etsuro Tanaka²⁾,
Hidezo Mori³⁾, Toshiaki Kawai⁴⁾, Haruo Obara⁵⁾, Toshio Ichimaru⁶⁾,
Kazuyoshi Takayama⁷⁾, Hideaki Ido⁸⁾

¹⁾ *Department of Physics, Iwate Medical University*

²⁾ *Department of Nutritional Science, Faculty of Applied Bio-science,
Tokyo University of Agriculture*

³⁾ *Department of Cardiac Physiology, National Cardiovascular Center Research Institute*

⁴⁾ *Electron Tube Division #2, Hamamatsu Photonics Inc.*

⁵⁾ *Department of Radiological Technology, College of Medical Science, Tohoku University*

⁶⁾ *Department of Radiological Technology, School of Health Sciences, Hirosaki University*

⁷⁾ *Shock Wave Research Center, Institute of Fluid Science, Tohoku University*

⁸⁾ *Department of Applied Physics and Informatics, Faculty of Engineering,
Tohoku Gakuin University*

Research Code No.: 200, 204.1

*Key Words: monochromatic radiography, quasi-parallel radiography, x-ray lens,
polycapillary plate*

Abstract

A fundamental study on quasi-parallel radiography using a polycapillary plate and a copper-target x-ray tube is described. In the experiments, the tube voltage was regulated from 12 to 22 kV, and the tube current was regulated within 3.0 mA by the filament temperature. The exposure time was controlled in order to obtain optimum x-ray intensity, and the maximum focal spot dimensions were approximately 2.0×1.5 mm. The thickness and the inner capillary tube diameter of the polycapillary were 1.0 mm and 25 μ m, respectively. Monochromatic x-rays were produced using a 10 μ m-thick nickel filter with a tube voltage of 17 kV, and these rays were formed into quasi-parallel beams by the polycapillary. The radiogram was taken using a computed

* 岩手医科大学教養部物理学科 [〒020-0015 岩手県盛岡市本町通3-16-1] : Department of Physics, Iwate Medical University
e-mail: msagae@iwate-med.ac.jp

radiography system utilizing imaging plates. In the measurement of image resolution, the spatial resolution hardly varied according to increases in the distance between the resolution-test chart and imaging plate using a polycapillary. A 50 μm tungsten wire could be observed, and fine blood vessels of approximately 100 μm were visible in angiography.

Received Jan. 7, 2004; revision accepted Jul. 5, 2004

1. Introduction

Monochromatic parallel radiography typically utilizes a synchrotron in conjunction with silicon single crystals and it has been applied in x-ray phase imaging¹⁻³⁾. It has also been applied in high contrast micro-angiography⁴⁻⁷⁾ because x-rays with energies of approximately 35 keV are absorbed effectively by the iodine-based contrast medium.

In order to produce monochromatic x-rays without using the synchrotron, we developed a molybdenum x-ray tube⁸⁾ with a transmission-type molybdenum target, which is used as a monochromatic filter for absorbing bremsstrahlung x-rays. In addition, from weakly ionized linear plasma, we found irradiations of intense and sharp characteristic x-rays⁹⁻¹²⁾.

Recently, several different x-ray lenses^{13,14)} have been developed, and a polycapillary plate⁸⁻¹⁵⁾ has been shown to be useful to perform quasi-parallel radiography with lower photon energy. For this, the plate thickness is about 1 mm, and it is very difficult to design a thicker plate due to technical limitation for increasing the straight capillary length.

In biomedical radiography, because the image processing can be done easily with a Computed Radiography (CR) system^{16,17)} utilizing imaging plates, the CR system is useful for monochromatic parallel radiography, regardless of whether the image resolution falls as compared with an x-ray film; the spatial resolution is primarily determined by the minimum sampling pitch of 87.5 μm .

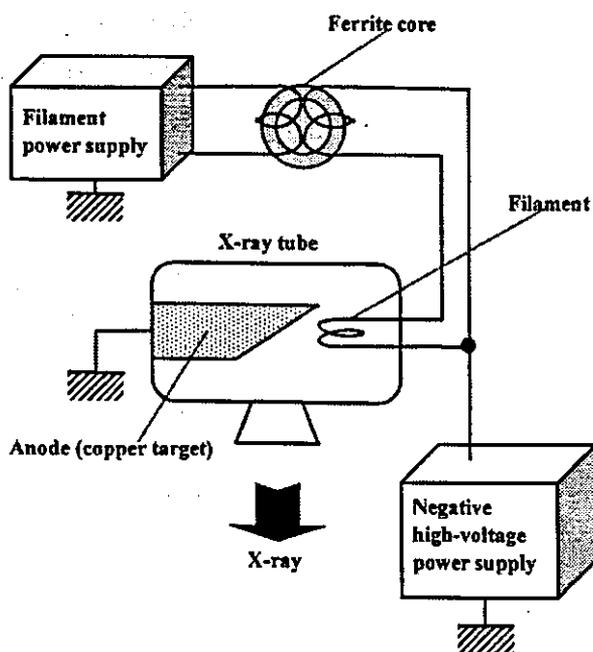


Fig. 1. Circuit diagram of the x-ray generator.

In this article, we describe a monochromatic quasi-parallel radiography system utilizing a polycapillary plate with an inner capillary diameter of 25 μm , a CR system, and a copper-target radiation tube to realize a low-priced x-ray system utilizing an x-ray lens.

2. Experimental setup

Figure 1 shows the circuit diagram of the x-ray generator, which consists of a negative high-voltage power supply, a filament (hot cathode) power supply, and a copper-target x-ray tube. The negative high voltage is applied to the cathode electrode, and the anode (target) is connected to the ground. In the experiments, the

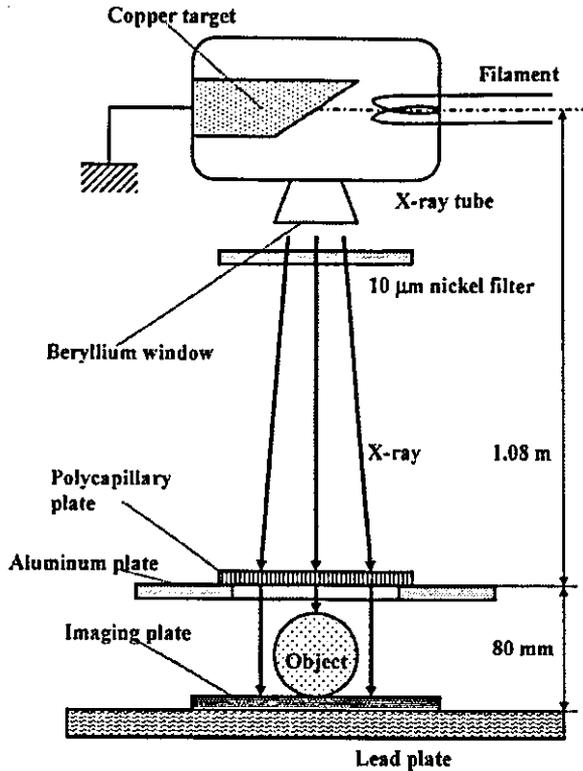
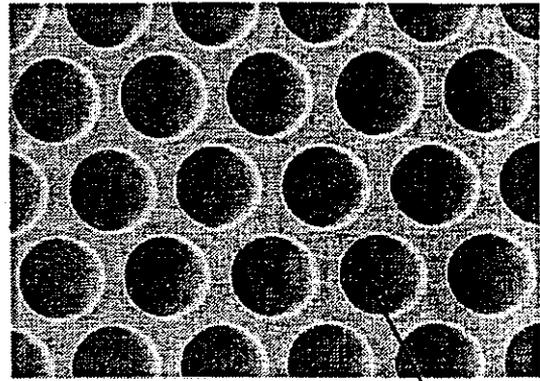


Fig. 2. Experimental setup for polycapillary imaging utilizing a CR system.

capillary imaging is shown in Fig. 2. Monochromatic x-rays were produced using a 10 μm -thick nickel filter, and these rays were formed into quasi-parallel beams by a polycapillary plate (Fig. 3). The polycapillary plate was J5022-21 (Hamamatsu Photonics Inc.), and the plate thickness was 1.0 mm. The outer, effective, and inner capillary diameters were 87 mm, 77 mm, and 25 μm , respectively. Radiography was performed by a CR system (Konica Regius 150) utilizing imaging plates. The distance between the x-ray source and the polycapillary was 1.08 m, and the polycapillary plate was set on an aluminum plate. The distance between the polycapillary and imaging plates was regulated by the height (30 mm) of the polymethyl methacrylate (PMMA) spacers used.



Capillary

Fig. 3. Polycapillary plate.

tube voltage was regulated from 12 to 22 kV, and the tube current was regulated by the filament temperature and ranged from 1.0 to 3.0 mA. The exposure time was controlled in order to obtain optimum x-ray intensity.

The experimental setup for performing poly-

capillary imaging is shown in Fig. 2. Monochromatic x-rays were produced using a 10 μm -thick nickel filter, and these rays were formed into quasi-parallel beams by a polycapillary plate (Fig. 3). The polycapillary plate was J5022-21 (Hamamatsu Photonics Inc.), and the plate thickness was 1.0 mm. The outer, effective, and inner capillary diameters were 87 mm, 77 mm, and 25 μm , respectively. Radiography was performed by a CR system (Konica Regius 150) utilizing imaging plates. The distance between the x-ray source and the polycapillary was 1.08 m, and the polycapillary plate was set on an aluminum plate. The distance between the polycapillary and imaging plates was regulated by the height (30 mm) of the polymethyl methacrylate (PMMA) spacers used.

3. Characteristics

3.1. Focal spot

In order to measure images of the x-ray source, we employed the CR system, a pinhole camera with a hole diameter of 50 μm , and a filter (Fig. 4). When the tube voltage was increased, the focal spot intensity increased; spot dimensions also increased slightly and were approximately 2.0×1.5 mm.

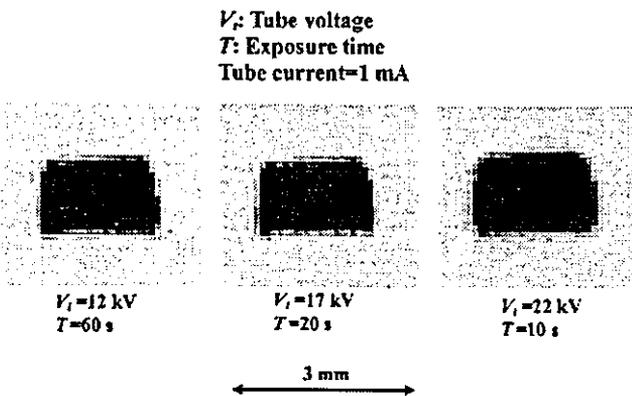


Fig. 4. Images of the x-ray source measured using a 50 μm -diameter pinhole while changing the tube voltage.

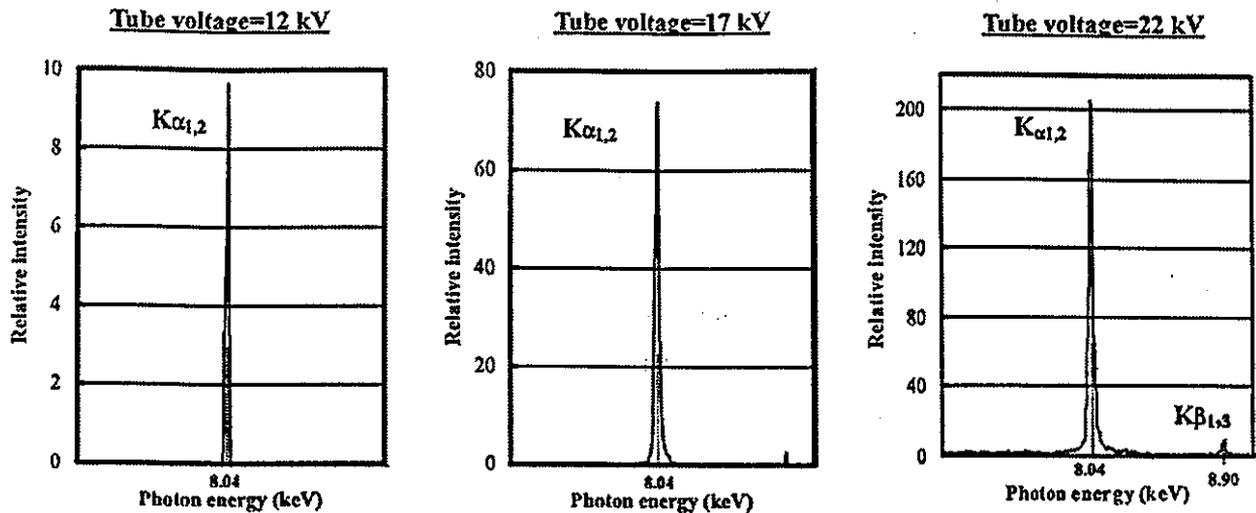


Fig. 5. Measured x-ray spectra while changing the tube voltage.

3.2. X-ray spectra

Monochromatic x-ray spectra from the copper-target tube were measured by a transmission-type spectrometer with a lithium fluoride curved crystal 0.5 mm in thickness. The spectra were taken by the CR system with a wide dynamic range, and relative x-ray intensity was calculated from Dicom digital data. Fig. 5 shows measured spectra from the copper target. When the tube voltage was increased, the characteristic x-ray intensity of $K\alpha$ lines increased.

4. Radiography

The monochromatic radiography was performed with a tube voltage of 17 kV using the filter. Figure 6 shows radiography for imaging a polycapillary plate, and radiograms of the polycapillary are shown in Fig. 7. The center of the black spot in the polycapillary radiogram was mainly imaged by direct transmission beams through capillary holes. As shown in this figure, the spot dimensions increased slightly according to decreases in the PMMA spacer height.

Radiography for imaging a test chart for determining image resolution, and the radio-

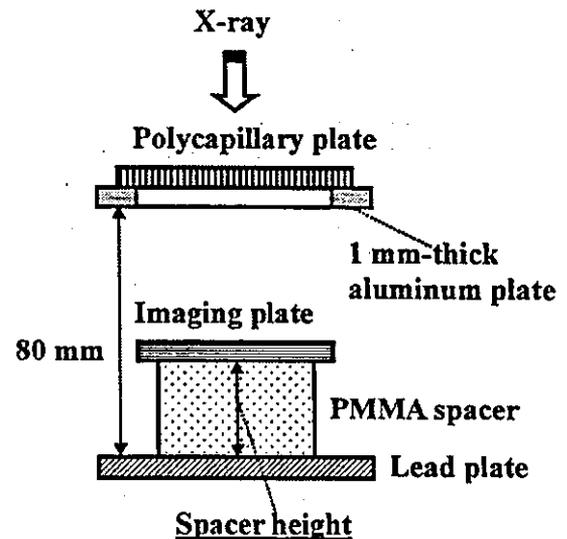


Fig. 6. Radiography for imaging a polycapillary plate while changing the distance between the polycapillary and imaging plates using PMMA spacers.

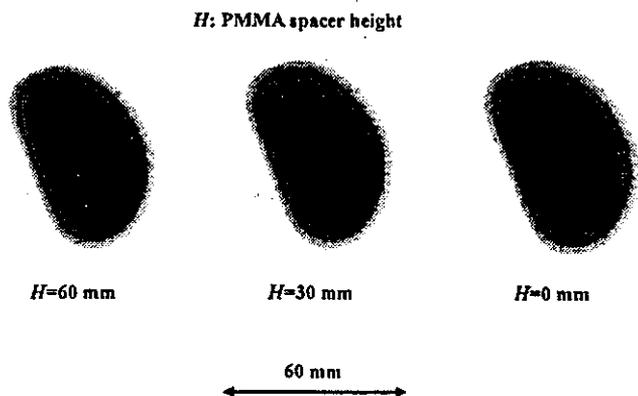


Fig. 7. Radiograms of a polycapillary plate while changing the PMMA height.

grams of $166\ \mu\text{m}$ width lead lines, are shown in Figs. 8 and 9, respectively. Both the image resolution and the line contrast fell with decreases in the spacer height. Figure 10 shows the polycapillary radiography for imaging the test chart; the polycapillary was set on the aluminum plate. With this radiography system, we obtained higher contrast lines as compared with those in Fig. 9. When the spacer height was increased, the image resolution hardly varied, and the image dimensions decreased slightly (Fig. 11).

Figures 12 and 13 show radiography and the radiogram of tungsten wires on a PMMA box, respectively. Although the image contrast increased with increases in the wire diameter, a $50\ \mu\text{m}$ -diameter wire could be observed. The angiography for a rabbit heart is shown in Fig 14; iodine-based microspheres of $15\ \mu\text{m}$ diameter were used, and fine blood vessels of about $100\ \mu\text{m}$ were visible (Fig. 15).

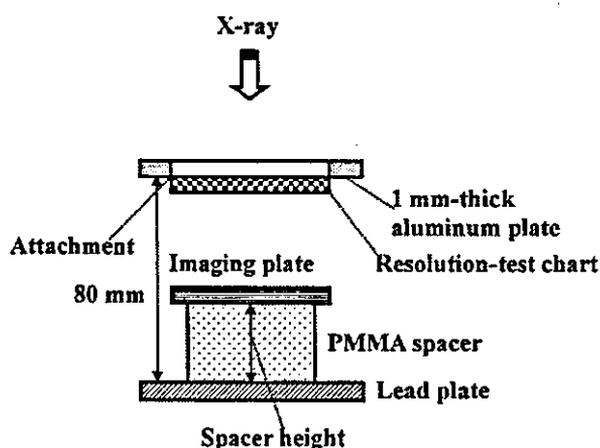


Fig. 8. Radiography for imaging a test chart according to the PMMA spacer height.

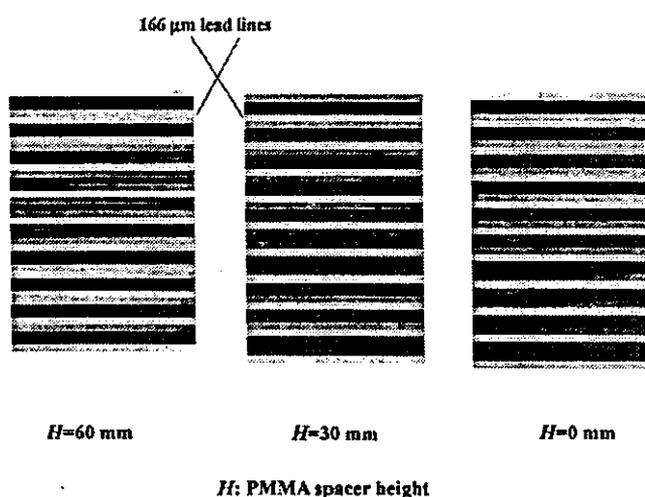


Fig. 9. Radiograms of a test chart according to the PMMA height.

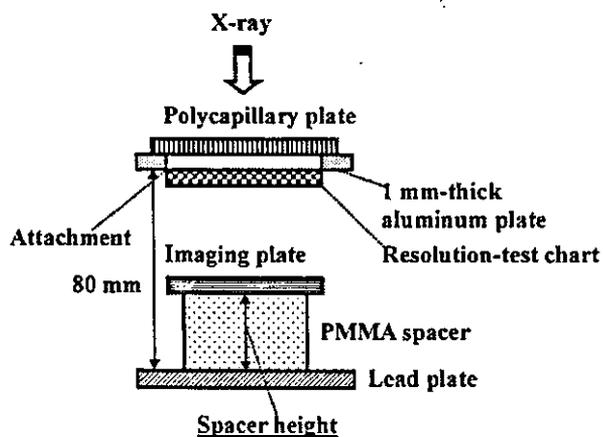


Fig. 10. Radiography for imaging a test chart using a polycapillary plate according to the PMMA height.

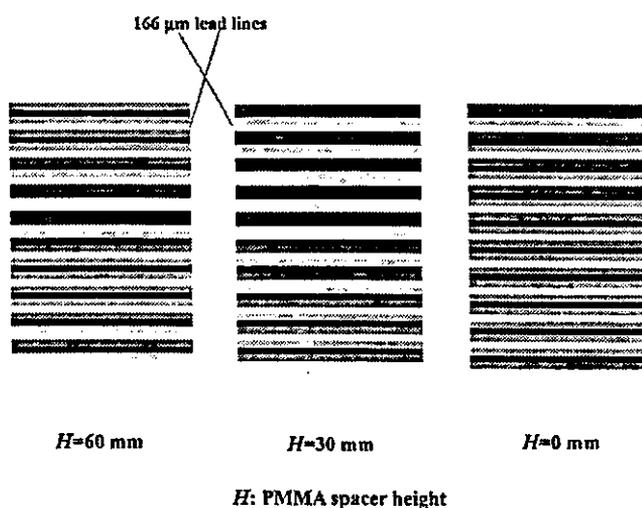


Fig. 11. Radiograms of a test chart using the polycapillary plate according to the PMMA height

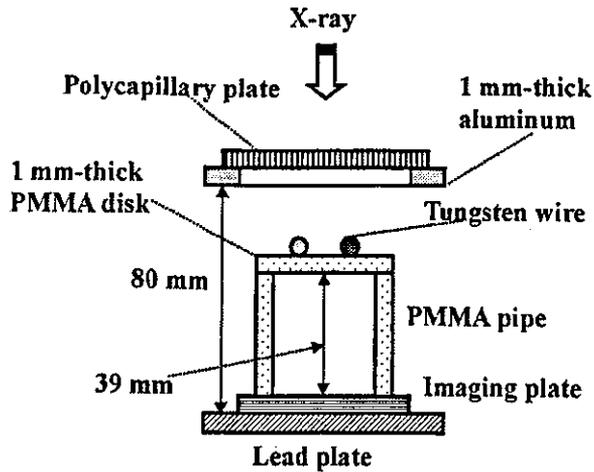


Fig. 12. Radiography for imaging tungsten wires using the polycapillary.

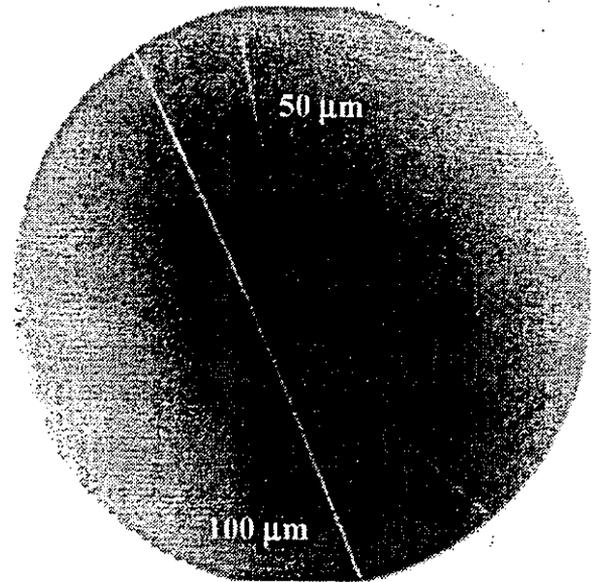


Fig. 13. Radiograms of tungsten wires on a PMMA spacer.

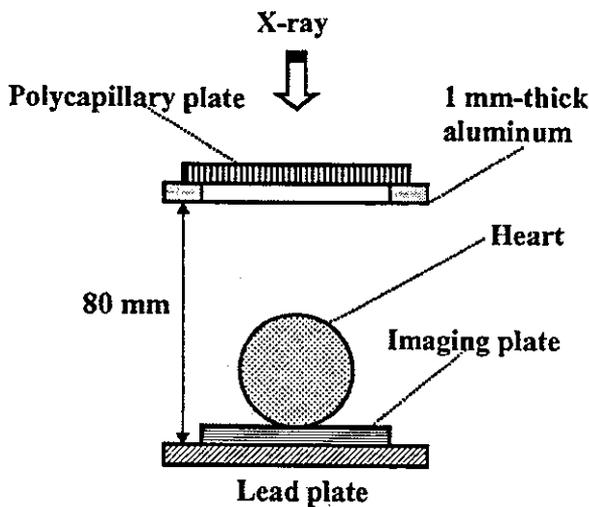


Fig. 14. Angiography using iodine-based microspheres of the heart extracted from a rabbit.

100 μm tungsten wire

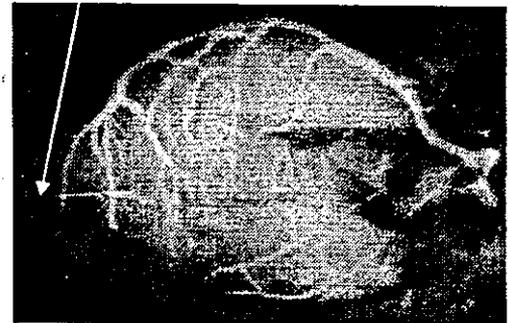


Fig. 15. Angiogram of the heart using the polycapillary.

5. Discussion

In this research, we carried out parallel radiography using a polycapillary plate in conjunction with monochromatic x-rays, and we obtained higher image resolutions as compared with those obtained without using the plate. Currently, the image resolution of the polycapillary is primarily determined by the inner capillary diameter and the thickness, and it is improved with decreases in the diameter and increases in the thickness. In cases where the CR system is employed, although the resolution of the CR system is primarily determined by the minimum sampling pitch of $87.5 \mu\text{m}$, we could observe $50 \mu\text{m}$ tungsten wires.

The photon energies of the characteristic x-rays are determined by the target element, and the capillary thickness should be increased according to increases in the photon energy because the transmission intensity through capillary glass increases. Subsequently, in order to increase the

parallelity for phase imaging, single crystals should be employed after passing the x-ray beam through the polycapillary.

Since it is possible to increase the irradiation field by increasing the distance between the x-ray source and the polycapillary, this system can be applied to image a wide variety of objects in various fields, including medical radiography.

Acknowledgments

This work was supported by Grants-in-Aid for Scientific Research (13470154, 13877114, and 16591222) and Advanced Medical Scientific Research from MECSST, Grants from Keiryō Research Foundation, The Promotion and Mutual Aid Corporation for Private Schools of Japan, JST (Test of Fostering Potential), NEDO, and MHLW (HLSRG, RAMT-nano-001, RHGTEFB-genome-005, and RGCD13C-1).

References

- 1) Davis T J, Gao D, Gureyev T E, et al.: Phase-contrast imaging of weakly absorbing materials using hard x-rays. *Nature* 373: 595-597, 1995
- 2) Momose A, Takeda T, Itai Y, et al.: Phase-contrast x-ray computed tomography for observing biological soft tissues. *Nature Medicine* 2: 473-475, 1996
- 3) Ishisaka A, Ohara H and Honda C: A new method of analyzing edge effect in phase contrast imaging with incoherent x-rays. *Opt. Rev.* 7: 566-572, 2000
- 4) Akisada A, Ando M, Hyodo K, Hasegawa S, et al.: An attempt at coronary angiography with a large size monochromatic SR beam. *Nucl. Instrum. Meth. Phys. Res. A*246: 713-718, 1986
- 5) Thompson A C, Zeman H D, Brown G S, et al.: First operation of the medical research facility at the NSLS for coronary angiography. *Rev. Sci. Instrum.* 63: 625-628, 1992
- 6) Mori H, Hyodo K, Tanaka E, et al.: Small-vessel radiography in situ with monochromatic synchrotron radiation. *Radiology* 201: 173-177, 1996
- 7) Hyodo K, Ando M, Oku Y, et al.: Development of a two-dimensional imaging system for clinical applications of intravenous coronary angiography using intense synchrotron radiation produced by a multipole wiggler. *J. Synchrotron Rad.* 5: 1123-1126, 1998
- 8) Sato E, Komatsu M, Hayasi Y, et al.: Quasi-monochromatic parallel radiography achieved with a plane-focus x-ray tube. *SPIE* 4786: 151-161, 2002
- 9) Sato E, Sagae M, Ichimaru T, et al.: Tentative study on x-ray enhancement by fluorescent emission of radiation by plasma x-ray source. *SPIE* 3771: 51-60, 1999
- 10) Sato E, Hayasi Y, Germer R, et al.: Intense characteristic x-ray irradiation from weakly ionized linear plasma and applications. *Jpn. J. Med. Imag. Inform. Sci.* 20: 148-155, 2003
- 11) Sato E, Hayasi Y, Germer R, et al.: Irradiation of intense characteristic x-rays from weakly ionized linear molybdenum plasma. *Jpn. J. Med. Phys.* 23: 123-131, 2003
- 12) Sato E, Hayasi Y, Germer R, et al.: Quasi-monochromatic flash x-ray generator utilizing weakly

- ionized linear copper plasma. Rev. Sci. Instrum. 74: 5236-5240, 2003
- 13) Xiao Q F and Poturaef S V: Polycapillary-based x-ray optics. Nucl. Instr. Meth. Phys. Res. A 347: 376-383, 1994
 - 14) MacDonald C A, Mail N, Li D, et al.: Monochromatic applications of polycapillary optics. SPIE 5196: 405-411, 2002
 - 15) Sato E, Germer R, Hayasi Y, et al.: Quasi-monochromatic parallel flash radiography achieved with a plane-focus x-ray tube. SPIE 4948: 646-651, 2002
 - 16) Sonoda M, Takano M, Miyahara J, et al.: Computed radiography utilizing scanning laser stimulated luminescence. Radiology 148: 833-838, 1983
 - 17) Sato E, Sato K and Tamakawa Y: Film-less computed radiography system for high-speed imaging. Ann. Rep. Iwate Med. Univ. Sch. Lib. Arts and Sci. 35: 13-23, 2000

Optimal Windows of Statin Use for Immediate Infarct Limitation

5'-Nucleotidase as Another Downstream Molecule of Phosphatidylinositol 3-Kinase

Shoji Sanada, MD, PhD; Hiroshi Asanuma, MD, PhD; Tetsuo Minamino, MD, PhD;
Koichi Node, MD, PhD; Seiji Takashima, MD, PhD; Hiroko Okuda, PhD;
Yoshiro Shinozaki, MD, PhD; Akiko Ogai, PhD; Masashi Fujita, MD; Akio Hirata, MD;
Jiyoung Kim, MD; Yoshihiro Asano, MD, PhD; Hidezo Mori, MD, PhD;
Hitonobu Tomoike, MD, PhD; Soichiro Kitamura, MD, PhD;
Masatsugu Hori, MD, PhD; Masafumi Kitakaze, MD, PhD

Background—Although statins are reported to have a cardioprotective effect, their immediate direct influence on ischemia-reperfusion injury and the underlying mechanisms remain obscure. We investigated these issues in an in vivo canine model.

Methods and Results—Dogs were subjected to coronary occlusion (90 minutes) and reperfusion (6 hours) immediately after injection of pravastatin (0.2, 2, or 10 mg/kg), pitavastatin (0.01, 0.1, or 0.5 mg/kg), or cerivastatin (0.5, 5, or 50 μ g/kg). Then myocardial phosphatidylinositol 3-kinase (PI3-K) and 5'-nucleotidase activities were measured, as well as infarct size. After 15 minutes of reperfusion, pravastatin caused dose-dependent activation of Akt and ecto-5'-nucleotidase in the ischemic zone, and the effect was significant at higher doses. Pitavastatin also significantly increased these activities, and its optimal dose was within the clinical range, whereas cerivastatin caused activation at the lowest dose tested. In all cases, both Akt and ecto-5'-nucleotidase showed activation in parallel, and this activation was completely abolished by wortmannin, a PI3-K inhibitor. The magnitude of the infarct-limiting effect paralleled the increase in Akt and ecto-5'-nucleotidase activity and was blunted by administration of wortmannin, α,β -methyleneadenosine-5'-diphosphate, or 8-sulfophenyltheophylline during reperfusion. Both collateral flow and the area at risk were comparable for all groups.

Conclusions—Activation of ecto-5'-nucleotidase after ischemia by PI3-K activation may be crucial for immediate infarct-size limitation by statins. There seems to be an optimal dose for each statin that is independent of its clinical cholesterol-lowering effect. (*Circulation*. 2004;110:2143-2149.)

Key Words: statins ■ myocardial infarction ■ adenosine ■ enzymes ■ phosphates

The 3-hydroxy-3-methylglutaryl coenzyme A reductase inhibitors (statins) block the biosynthesis of cholesterol¹ and are widely used clinically to decrease serum cholesterol levels. Recent studies have focused on the pleiotropic effects of either hydrophilic^{2,3} or hydrophobic^{4,5} statins, which are independent of their cholesterol-lowering effect.^{2,3,5} Protection against ischemia-reperfusion injury is one of them, which is particularly evident after 12 hours.^{6,7} In addition, some studies showed that statins activate the phosphatidylinositol 3-kinase (PI3-K)/Akt pathway within 1 hour,^{8,9} as well as activating endothelial nitric oxide synthase (eNOS),^{9,10} to cause immediate infarct limitation.⁷

On the other hand, other studies revealed that statins also acutely activate ecto-5'-nucleotidase,¹¹ which produces the endogenous cardioprotective substance adenosine,¹² especially in response to certain stresses.¹³ Ecto-5'-nucleotidase can act only when localized on the cell membrane,¹³ and the density of this enzyme on the membrane regulates its activity.^{11,14} Endocytotic turnover of ecto-5'-nucleotidase (5'-nucleotidase localized on the cell surface) is inhibited by PI3-K activation,¹⁴ which subsequently increases total 5'-nucleotidase activity within a period as short as 10 minutes.¹⁴ Therefore, we hypothesized that an increase of ecto-5'-nucleotidase activity might be critical for early cardioprotec-

Received March 26, 2004; revision received May 4, 2004; accepted May 7, 2004.

From the Department of Internal Medicine and Therapeutics (S.S., H.A., T.M., S.T., H.O., M.F., A.H., Y.A., M.H.), Osaka University Graduate School of Medicine, Suita; the Department of Cardiovascular and Renal Medicine (K.N.), Saga University Faculty of Medicine, Saga; the Department of Physiological Science (Y.S.), Tokai University School of Medicine, Isehara; and the Cardiovascular Division of Medicine (A.O., J.K., H.M., H.T., S.K., M.K.), National Cardiovascular Center, Suita, Japan.

Correspondence to Masafumi Kitakaze, MD, PhD, Director, Cardiovascular Division of Medicine, National Cardiovascular Center, 5-7-1 Fujishirodai, Suita, 565-8565 Japan. E-mail: kitakaze@zf6.so-net.ne.jp

© 2004 American Heart Association, Inc.

Circulation is available at <http://www.circulationaha.org>

DOI: 10.1161/01.CIR.0000143830.59419.73

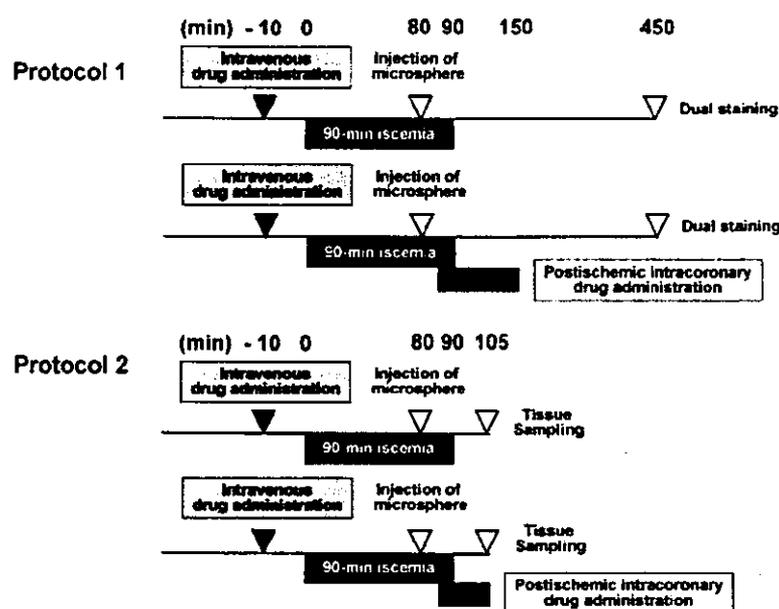


Figure 1. Experimental protocols to measure infarct size (protocol 1; Upper) and kinase activity (protocol 2; Lower).

tion mediated by statins and might be associated with rapid activation of PI3-K.

Here we used a dog model to determine whether 3 statins with different water solubilities (pravastatin, pitavastatin, and cerivastatin) could acutely limit infarct size, as well as whether adenosine and PI3-K were involved in the underlying mechanism.

Methods

All procedures were performed in conformity with the *Guide for the Care and Use of Laboratory Animals* (NIH publication No. 85-23, 1996 revision) and were approved by the Osaka University Committee for Laboratory Animal Use. Pravastatin, pitavastatin, and cerivastatin were obtained from Sankyo, Kowa, and Takeda Pharmaceuticals, respectively. The other drugs were obtained from Sigma.

Instrumentation

Beagle dogs weighing 8 to 13 kg were anesthetized and connected to an extracorporeal bypass tube as described previously.^{15,16} In all experiments, the average baseline values of mean aortic blood pressure (ABP), heart rate (HR), and arterial blood P_{O_2} were 102 ± 2.2 mm Hg, 129 ± 2.5 min^{-1} , and 109 ± 4.1 mm Hg, respectively. Both ABP and HR were measured continuously during the study.

Experimental Protocols

Protocol 1: Measurement of Infarct Size and Myocardial Collateral Blood Flow

After hemodynamic stabilization, we infused pravastatin (0.2, 2, or 10 mg/kg), pitavastatin (0.01, 0.1, or 0.5 mg/kg), cerivastatin (0.5, 5, or 50 $\mu\text{g}/\text{kg}$) or saline intravenously for 10 minutes before 90 minutes of sustained ischemia, which was followed by 6 hours of reperfusion ($n=9$ to 13 each). Some groups also received intracoronary administration of a selective ecto-5'-nucleotidase inhibitor (α,β -methyleneadenosine-5'-diphosphate [AMP-CP; 80 $\mu\text{g} \cdot \text{kg}^{-1} \cdot \text{min}^{-1}$]); a nonselective adenosine receptor antagonist (8-sulfophenyltheophylline [8-SPT; 50 $\mu\text{g} \cdot \text{kg}^{-1} \cdot \text{min}^{-1}$]); or a selective PI3-K inhibitor (wortmannin [1.5 $\mu\text{g} \cdot \text{kg}^{-1} \cdot \text{min}^{-1}$]) between 5 minutes before and 60 minutes after reperfusion. We measured infarct size and regional myocardial collateral blood flow during 90 minutes of ischemia as described previously.¹⁵

We have already confirmed in the same model that the doses of AMP-CP,¹⁷ 8-SPT,^{17,18} or wortmannin¹⁹ used in this study were appropriate to block ecto-5'-nucleotidase, the adenosine receptors, or PI3-K, respectively. Figure 1 shows the details of this protocol, and the Table lists all of the groups studied.

Protocol 2: Myocardial Enzyme Assays

Another 54 dogs underwent a procedure identical to that of some groups from protocol 1 and were studied for enzyme assays ($n=3$ or 4 each). In this protocol, not only wortmannin (1.5 $\mu\text{g} \cdot \text{kg}^{-1} \cdot \text{min}^{-1}$) but also LY294002 (60 $\mu\text{g} \cdot \text{kg}^{-1} \cdot \text{min}^{-1}$) was used as another selective PI3-K inhibitor. After 15 minutes of reperfusion, a myocardial tissue sample was obtained from the ischemic border zone to ensure evaluation of viable ischemic myocardium and was used for the measurement of PI3-K and ecto-/endo-5'-nucleotidase activity. The myocardial tissue was rapidly frozen in LN_2 and stored at -80°C . Measurement of PI3-K and 5'-nucleotidase activity was done as reported previously^{15,19} with minor modifications.

Criteria for Exclusion

To ensure that all of the animals included in analysis were healthy and were exposed to a similar extent of ischemia, the exclusion criteria reported previously¹⁶ for hemodynamics, excessive collateral flow, and lethal arrhythmia were adopted.

Statistical Analysis

Results were expressed as mean \pm SEM, and the number of animals or experiments is shown as n . Statistical analysis was performed by ANOVA with a modified Bonferroni post hoc test, and significance was defined at $P < 0.05$.

Results

Mortality and Exclusions in Protocol 1

Among 222 dogs used in protocols 1, 56 dogs met the exclusion criteria of ventricular fibrillation or excessive myocardial collateral blood flow (>15 $\text{mL} \cdot 100$ $\text{g}^{-1} \cdot \text{min}^{-1}$). Therefore, 166 dogs completed these protocols satisfactorily and were included in the data analysis (Table).

Changes in Hemodynamic Parameters, Risk Area, and Collateral Blood Flow in Protocol 1

The changes in ABP and HR were comparable among all groups throughout the protocol (data not shown), and both the

TABLE 1. Mortality, Exclusion, Area at Risk, and Collateral Flow in Each Group in Protocol 1

Groups	Excluded						
	Lethal Arrhythmia				Final No.	Area at Risk, %	Collateral Flow, mL/100 g per minute
	Initial No.	During 1 ischemia	After Reperfusion	Excessive Collateral Flow			
Control	13	1	2	1	9	40.1±2.1	8.2±1.0
Prava							
0.2	9	0	1	0	8	38.8±2.0	8.4±1.2
2.0	10	0	0	2	8	39.1±2.2	8.9±1.1
10	10	0	0	2	8	39.6±2.1	8.9±1.4
Pitava							
0.01	9	1	1	0	7	38.7±2.2	8.1±1.3
0.1	11	0	1	2	8	39.3±2.0	9.2±1.5
0.5	10	1	0	2	7	39.9±1.9	8.8±1.5
Ceriva							
0.5	11	0	1	2	8	39.2±1.9	8.5±1.3
5.0	10	1	1	1	7	38.9±2.1	8.7±1.4
50	11	0	1	3	7	39.0±2.0	9.1±1.5
AMP-CP							
-Prava 10	9	0	2	0	7	40.4±2.3	8.6±1.3
+Pitava 0.1	9	0	1	1	7	39.8±2.0	8.4±1.5
+Ceriva 0.5	9	1	1	0	7	40.4±2.3	9.0±1.4
8SPT							
+Prava 10	10	0	1	1	8	38.7±2.2	8.3±1.3
+Pitava 0.1	11	1	2	0	8	39.9±2.1	8.2±1.6
+Ceriva 0.5	11	0	2	1	8	38.4±2.6	8.5±1.5
WTMN							
+Prava 10	10	0	2	1	7	38.6±2.3	9.5±1.5
+Pitava 0.1	10	0	2	0	8	38.9±2.1	9.2±1.6
-Ceriva 0.5	10	0	1	1	8	39.8±2.8	8.8±1.4
AMP-CP	9	0	2	0	7	38.8±2.5	8.5±1.6
8SPT	11	0	3	0	8	39.6±2.5	8.2±1.5
WTMN	9	1	2	0	6	40.5±2.3	8.6±1.6

Data expressed as mean±SEM. Prava indicates pravastatin (mg/kg); Pitava, pitavastatin (mg/kg); Ceriva, cerivastatin (μ g/kg); 8SPT, 8-sulfophenyltheophylline; and WTMN, wortmannin.

area at risk and collateral blood flow were also comparable (Table).

Infarct Size

Figure 2 shows infarct size in the groups of protocol 1. Pravastatin (0.2, 2, and 10 mg/kg) dose-dependently reduced the infarct size (29.5±3.5%, 22.5±4.0%, and 18.8±3.4%, respectively) compared with that in the control group (39.8±3.6%), and the difference was significant at 2 mg/kg or more. Pitavastatin (0.01, 0.1, and 0.5 mg/kg) also reduced infarct size (32.9±3.9%, 23.6±3.8%, and 31.4±3.9%, respectively), although the optimal dose was 0.1 mg/kg (the only dose that produced a significant difference). Although cerivastatin (0.5, 5, and 50 μ g/kg) caused infarct limitation (26.2±3.2%, 32.1±5.3%, and 37.1±4.4%, respectively), it was significant at the lowest dose only, and the effect was

weaker at higher doses. Furthermore, cotreatment with AMP-CP, 8-SPT, or wortmannin between 5 minutes before and 60 minutes after reperfusion abrogated the infarct-limiting effect of pravastatin (39.9±4.0%, 42.6±4.0%, or 38.6±3.6%, respectively), pitavastatin (40.4±3.1%, 39.4±3.6%, or 39.1±3.1%, respectively), and cerivastatin (41.1±3.7%, 42.1±3.9%, or 40.4±4.0%, respectively), although these drugs per se did not affect infarct size (42.7±4.5%, 40.3±3.5%, or 42.7±4.5%, respectively).

5'-Nucleotidase Activity at Reperfusion

Figure 3 shows the activity of ecto-/endo-5'-nucleotidase in protocol 2. Sustained ischemia for 90 minutes and 15 minutes of subsequent reperfusion did not significantly change the activity of ecto-5'-nucleotidase (41.0±5.7 versus 33.2±1.2 nmol·mg protein⁻¹·min⁻¹ at baseline). Preischemic treat-

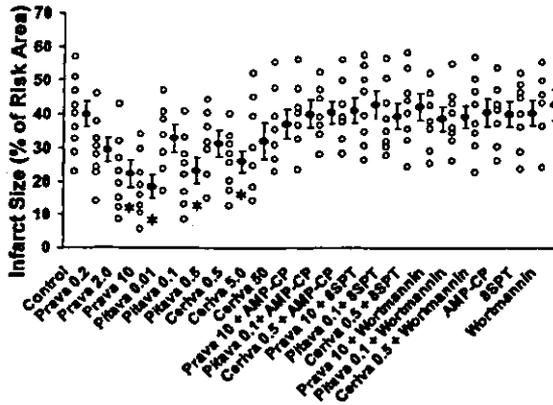


Figure 2. Infarct size in each group in protocol 1. Data are expressed as mean \pm SEM. * $P < 0.05$ vs control. Open circles show infarct size in each individual. Prava indicates pravastatin; Pitava, pitavastatin; and Ceriva, cerivastatin. All other abbreviations are as defined in text.

ment with pravastatin caused a dose-dependent and acute increase of ecto-5'-nucleotidase activity in the ischemic zone, which became significant at the highest dose (72.6 ± 6.0 nmol \cdot mg protein $^{-1}$ \cdot min $^{-1}$ at 10 mg/kg, $P < 0.05$ versus control). Pitavastatin also caused significant activation at its optimal (medium) dose (66.7 ± 6.1 nmol \cdot mg protein $^{-1}$ \cdot min $^{-1}$ at 0.1 mg/kg, $P < 0.05$ versus control). Cerivastatin caused activation at the lowest dose (62.5 ± 5.6 nmol \cdot mg protein $^{-1}$ \cdot min $^{-1}$ at 0.5 μ g/kg, $P < 0.05$ versus control). All of these increases were canceled by the selective PI3-K inhibitors wortmannin (39.5 ± 6.8 nmol \cdot mg protein $^{-1}$ \cdot min $^{-1}$ for pravastatin, 37.0 ± 7.1 nmol \cdot mg protein $^{-1}$ \cdot min $^{-1}$ for pitavastatin, and 38.4 ± 6.5 nmol \cdot mg protein $^{-1}$ \cdot min $^{-1}$ for cerivastatin) or LY294002 (33.5 ± 6.5 nmol \cdot mg protein $^{-1}$ \cdot min $^{-1}$ for pravastatin, 35.0 ± 6.2 nmol \cdot mg protein $^{-1}$ \cdot min $^{-1}$ for pitavastatin, and 37.5 ± 6.7 nmol \cdot mg

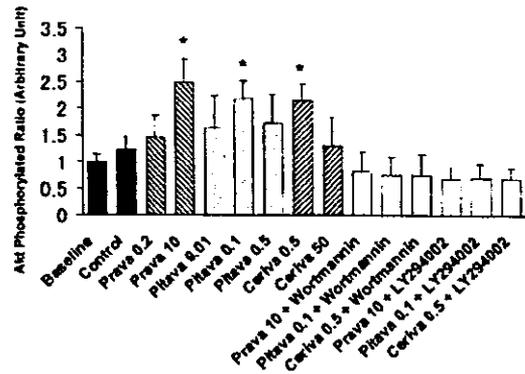


Figure 4. Myocardial PI3-K activity represented by phosphorylated ratio of Akt in each group in protocol 2. Data are expressed as mean \pm SEM. n=4 each, * $P < 0.05$ vs control. Abbreviations are as defined in text and in legend to Figure 2.

protein $^{-1}$ \cdot min $^{-1}$ for cerivastatin). The activity of endo-5'-nucleotidase remained unchanged in all cases.

PI3-K Activity at Reperfusion

Figure 4 shows the activity of PI3-K in protocol 2. Sustained ischemia for 90 minutes and subsequent reperfusion for 15 minutes did not change PI3-K activity significantly ($123 \pm 23\%$ versus $100 \pm 14\%$ at baseline). Preischemic treatment with pravastatin caused dose-dependent and acute activation of ecto-5'-nucleotidase in the ischemic zone, which was significant at the highest dose ($249 \pm 44\%$ at 10 mg/kg, $P < 0.05$ versus control). Pitavastatin also caused significant activation at its medium dose ($218 \pm 34\%$ at 0.1 mg/kg, $P < 0.05$ versus control), whereas cerivastatin caused activation at the lowest dose ($214 \pm 31\%$ at 0.5 μ g/kg, $P < 0.05$ versus control). We confirmed that all of these increases were also blocked by wortmannin ($81 \pm 38\%$ for pravastatin,

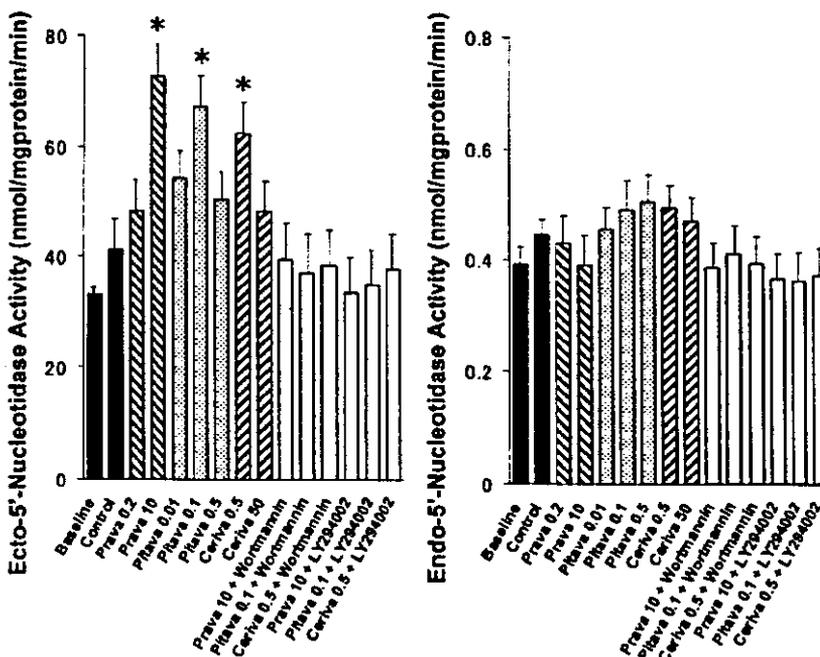


Figure 3. Myocardial ecto-/endo-5'-nucleotidase activity in each group in protocol 2. Data are expressed as mean \pm SEM. n=4 each, * $P < 0.05$ vs control. Abbreviations are as defined in text and in legend to Figure 2.

77±32% for pitavastatin, and 76±39% for cerivastatin) or LY294002 (69±23% for pravastatin, 70±27% for pitavastatin, and 68±21% for cerivastatin).

Discussion

The present study demonstrates that several statins provide immediate infarct limitation of different magnitudes and at different optimal doses. Our results also suggest that activation of ecto-5'-nucleotidase through the activation of PI3-K after ischemia was involved in this cardioprotective mechanism of statins.

Cholesterol-Lowering Effects and Immediate Infarct Limitation of Statins

In this study, we set the doses of statins in line with their clinical cholesterol-lowering properties. In Japan, the standard clinical doses to obtain a 20% to 30% reduction of total plasma cholesterol levels were 10 mg/d for pravastatin, 2 mg/d for pitavastatin, and 0.15 mg/d for cerivastatin. Our preliminary trials in the same dog model revealed that a single intravenous injection of 0.2 mg/kg pravastatin, 0.1 mg/kg pitavastatin, or 5 µg/kg cerivastatin approximated the clinical cholesterol-lowering dose based on the maximal plasma concentration of each statin (data not shown). Because (1) the maximal infarct limitation was achieved by a higher dose of pravastatin than the clinical dose, whereas the dose was similar to the clinical dose for pitavastatin and lower for cerivastatin, and (2) these statins showed early cardioprotection within 2 hours of administration in this model, it is strongly suggested that the magnitude of immediate infarct limitation by each statin is not correlated with its cholesterol-lowering effect.

Existence of Optimal Cardioprotective Doses for Each Statin

In the present report, we have directly shown that pitavastatin has the optimal dose to reduce infarct size. Obviously, there is also an optimal dose for cerivastatin under the lowest dose we tried, because infarct size with far lower doses of cerivastatin near zero will converge with those of control levels. In the case of pravastatin, our additional experiment, within the limitation with regard to the total amount of the drug we could obtain, showed that 100 mg/kg pravastatin administered in the same manner as in protocol 1 exerted similar (but a slightly weaker) magnitude of reducing infarct size (20.9±4.5%, n=5) compared with that achieved with 10 mg/kg of this agent. Although we could not show direct evidence in this case, it would at least not deny the possibility for the existence of an optimal dose of pravastatin. Furthermore, other reports also showed the existence of an optimal dose of atorvastatin for infarct limitation⁹ or of simvastatin for PI3-K activation.⁸ Taken together, the existence of optimal doses should be ubiquitous among all (or at least all hydrophobic) statins.

Although direct exhibition of the reason for this phenomenon remains unclear in this study, there might be some reasons to regulate the respective optimal windows for each statin, eg, differences in the ability to attenuate inflammatory response²⁰ or in the potency of direct absorption into cellular

membrane to modulate intracellular signaling systems. In addition, our present finding that infarct limitation completely paralleled the activation of PI3-K leads us to hypothesize that the lesser effects by the higher doses of statins should be regulated upstream of PI3-K. One possibility is that all hydrophobic statins can dose-dependently activate apoptosis-related signals,²¹ which might also explain the wide range of higher cardioprotective doses for pravastatin specifically. Finally, additional studies will need to be performed to obtain direct evidence.

Cardioprotective Mechanisms

Our observations that (1) activation of PI3-K and ecto-5'-nucleotidase was coincident with a substantial limitation of infarct size, (2) either wortmannin or AMP-CP abolished cardioprotection by all 3 statins, (3) different PI3-K inhibitors at reperfusion actually inhibited PI3-K activity (Figure 4) and subsequently reduced ecto-5'-nucleotidase activity (Figure 3), and (4) our preliminary documentation that PI3-K inhibition by either wortmannin or LY294002 before ischemia did not abolish the infarct limitation by statins in the present study (n=4 or 5, data not shown), together suggest that infarct limitation in this model was linked to the activation of PI3-K during reperfusion, not before ischemia, followed by ecto-5'-nucleotidase activation.

In this study, we did not determine the exact mechanism of how PI3-K activates ecto-5'-nucleotidase. Although we have previously reported that phosphorylation of ecto-5'-nucleotidase might be crucial,²² other mechanisms may also be involved, such as endocytotic turnover.¹⁷ In addition, although we did not evaluate real-time regional myocardial production of adenosine in each group, treatment with a potent adenosine receptor antagonist (8-SPT) during reperfusion also blunted infarct limitation by statins along with the inhibition of ecto-5'-nucleotidase, further suggesting that cardioprotection against ischemia-reperfusion injury via ecto-5'-nucleotidase activation might be mediated by an increase of adenosine, the main product of ecto-5'-nucleotidase.^{11,13,22} However, other implicated mechanism of enhanced activation of the adenosine receptor (eg, increased receptor sensitivity) should be determined by future studies.

Possible Link Between Cardioprotection by Adenosine and NO

Previous studies support our present findings that statins rapidly activate the PI3-K/Akt pathway,^{8,9} and we obtained another preliminary finding that the cotreatment with *N*^G-nitro-L-arginine methyl ester (10 µg · kg⁻¹ · min⁻¹) in the same manner as in protocol 1, which we confirmed did not affect baseline infarct size in the present model,²³ blunted the infarct limitation by pravastatin (36.8±4.1%, n=7), pitavastatin (39.9±3.9%, n=6), and cerivastatin (42.6±4.6%, n=5). Therefore, there is a possibility that ecto-5'-nucleotidase and NO act in series to cause statin-induced cardioprotection.

Although elucidation of a direct effect should be the focus of future studies, there are at least 2 lines of evidence to support the explanation that adenosine and NO synergistically caused infarct limitation in this study. First, NO directly exerts cardioprotection²⁴; NO inhibits cell-to-cell adhesion,

such as that between platelets²⁵ or between neutrophils and endothelial cells,^{26,27} by reducing expression of P-selectin,²⁷ E-selectin, and intercellular adhesion molecule-1,²⁸ which leads to attenuation of the inflammatory response^{22,24,25} or protects against ischemia-reperfusion injury.^{25–28} In addition, NO is reported to inhibit caspase-3 activity and to block apoptosis of cardiac myocytes.²⁹ On the other hand, adenosine also rescues injured myocardium through activating adenosine receptors.^{13,30–32} Either administration of adenosine or enhancement of endogenous adenosine release during reperfusion after sustained ischemia limits infarct size.^{13,17} We and others have shown that (1) adenosine receptor (A₁ and A₂) activation improves contractile dysfunction after reperfusion,¹⁴ (2) inhibition of norepinephrine release from the presynaptic vesicles and attenuation of calcium influx occur through the A₁ receptor and the coupled inhibitory G protein,^{33,34} (3) inhibition of platelet aggregation and leukocyte activation occurs through the A₂ receptor and the coupled stimulatory G protein,^{34–36} and (4) activation of extracellular signal-regulated kinase, one of the reperfusion injury survival kinase pathways,³⁷ takes place during reperfusion through the A₃ receptor.³⁸ Therefore, either adenosine or NO similarly and potentially protects injured myocardium through multiple pathways.

Second, recent articles have shown that either adenosine^{35–40} or NO⁴¹ can reactivate PI3-K downstream. However, increasing the production of both agents is known to negatively regulate further increases of production of these molecules,^{42,43} suggesting the requirement of both pathways to confer sufficient cardioprotection in the physiological system. Taking all of these together, it is likely that adenosine and NO synergistically confer the statin-derived immediate cardioprotection shown in this study.

In conclusion, our findings suggest the cellular mechanism by which statins attenuate myocardial injury, which may indicate the possibility of acute protective therapies for ischemia and associated myocardial stresses.

Acknowledgments

This study was supported by grants on the Human Genome, Tissue Engineering and Food Biotechnology (H13-Genome-11) and grants on Comprehensive Research on Aging and Health (H13-21seiki[seikatsu]-23) in Health and Labor Sciences Research from the Ministry of Health, Labor and Welfare; a grant-in-aid for Scientific Research from the Ministry of Education, Culture, Sports, Science and Technology of Japan; and in part by a grant-in-aid for JSPS fellows from the Japan Society for the Promotion of Science and the Japan Heart Foundation.

References

- Goldstein JL, Brown MS. Regulation of the mevalonate pathway. *Nature*. 1990;343:425–430.
- Sacks FM, Pfeffer MA, Moye LA, et al. The effect of pravastatin on coronary events after myocardial infarction in patients with average cholesterol levels: Cholesterol and Recurrent Events Trial investigators. *N Engl J Med*. 1996;335:1001–1009.
- LIPID Study Group. Prevention of cardiovascular events and death with pravastatin in patients with coronary heart disease and a broad range of initial cholesterol levels: the Long-Term Intervention with Pravastatin in Ischaemic Disease (LIPID) Study Group. *N Engl J Med*. 1998;339:1349–1357.
- 4S Study Group. Randomized trial of cholesterol lowering in 4444 patients with coronary heart disease: the Scandinavian Simvastatin Survival Study (4S). *Lancet*. 1994;344:1383–1389.
- Downs JR, Clearfield M, Weis S, et al. Primary prevention of acute coronary events with lovastatin in men and women with average cholesterol levels: results of AFCAPS/TexCAPS: Air Force/Texas Coronary Atherosclerosis Prevention Study. *JAMA*. 1998;279:1615–1622.
- Lefer AM, Campbell B, Shin YK, et al. Simvastatin preserves the ischemic-reperfused myocardium in normocholesterolemic rat hearts. *Circulation*. 1999;100:178–184.
- Ikeda Y, Young LH, Lefer AM. Rosuvastatin, a new HMG-CoA reductase inhibitor, protects ischemic reperfused myocardium in normocholesterolemic rats. *J Cardiovasc Pharmacol*. 2003;41:649–656.
- Kureishi Y, Luo Z, Shiojima I, et al. The HMG-CoA reductase inhibitor simvastatin activates the protein kinase Akt and promotes angiogenesis in normocholesterolemic animals. *Nat Med*. 2000;6:1004–1010.
- Bell RM, Yellon DM. Atorvastatin, administered at the onset of reperfusion, and independent of lipid lowering, protects the myocardium by up-regulating a pro-survival pathway. *J Am Coll Cardiol*. 2003;41:508–515.
- Simoncini T, Genazzani AR, Liao JK. Nongenomic mechanisms of endothelial nitric oxide synthase activation by the selective estrogen receptor modulator raloxifene. *Circulation*. 2002;105:1368–1373.
- Ledoux S, Laouari D, Essig M, et al. Lovastatin enhances ecto-5'-nucleotidase activity and cell surface expression in endothelial cells: implication of rho-family GTPases. *Circ Res*. 2002;90:420–427.
- Kitakaze M, Hori M, Morioka T, et al. α -Adrenoceptor activation mediates the infarct size-limiting effect of ischemic preconditioning through augmentation of 5'-nucleotidase activity. *J Clin Invest*. 1994;93:2197–2205.
- Kitakaze M, Minamino T, Node K, et al. Adenosine and cardioprotection in the diseased heart. *Jpn Circ J*. 1999;63:231–243.
- Tuma PL, Finnegan CM, Yi JH, et al. Evidence for apical endocytosis in polarized hepatic cells: phosphoinositide 3-kinase inhibitors lead to the lysosomal accumulation of resident apical plasma membrane proteins. *J Cell Biol*. 1999;145:1089–1102.
- Kitakaze M, Node K, Minamino T, et al. Role of activation of protein kinase C in the infarct size-limiting effect of ischemic preconditioning through activation of ecto-5'-nucleotidase. *Circulation*. 1996;93:781–791.
- Sanada S, Kitakaze M, Papst PJ, et al. Role of phasic dynamism of p38 mitogen-activated protein kinase activation in the ischemic preconditioning on the canine heart. *Circ Res*. 2001;88:175–180.
- Kitakaze M, Minamino T, Funaya H, et al. Vesnarinone limits infarct size via adenosine-dependent mechanisms in the canine heart. *Circulation*. 1997;95:2108–2114.
- Node K, Kitakaze M, Minamino T, et al. Activation of ecto-5'-nucleotidase by protein kinase C and its role in ischaemic tolerance in the canine heart. *Br J Pharmacol*. 1997;120:273–281.
- Ogita H, Node K, Asanuma H, et al. Raloxifene improves coronary perfusion, cardiac contractility and myocardial metabolism in the ischemic heart: role of phosphatidylinositol 3-kinase/Akt pathway. *J Cardiovasc Pharmacol*. 2004;43:821–829.
- Hilgendorff A, Muth H, Parviz B, et al. Statins differ in their ability to block NF- κ B activation in human blood monocytes. *Int J Clin Pharmacol Ther*. 2003;41:397–401.
- Kaneta S, Satoh K, Kano S, et al. All hydrophobic HMG-CoA reductase inhibitors induce apoptotic death in rat pulmonary vein endothelial cells. *Atherosclerosis*. 2003;170:237–243.
- Kitakaze M, Minamino T, Node K, et al. Activation of ecto-5'-nucleotidase and cardioprotection of ischemic preconditioning. *Basic Res Cardiol*. 1996;91:23–26.
- Asanuma H, Kitakaze M, Funaya H, et al. Nifedipine limits infarct size via NO-dependent mechanisms in dogs. *Basic Res Cardiol*. 2001;96:497–505.
- Lefer AM, Lefer DJ. Nitric oxide. II: nitric oxide protects in intestinal inflammation. *Am J Physiol*. 1999;276:G572–G575.
- Massberg S, Sausbier M, Klatt P, et al. Increased adhesion and aggregation of platelets lacking cyclic guanosine 3',5'-monophosphate kinase I. *J Exp Med*. 1999;189:1255–1264.
- Agullo L, Garcia-Dorado D, Insero J, et al. L-Arginine limits myocardial cell death secondary to hypoxia-reoxygenation by a cGMP-dependent mechanism. *Am J Physiol*. 1999;276:H1574–H1580.

27. Jordan JE, Zhao ZQ, Vinten-Johansen J. The role of neutrophils in myocardial ischemia-reperfusion injury. *Cardiovasc Res.* 1999;43:860–878.
28. Buras JA, Stahl GL, Svoboda KK, et al. Hyperbaric oxygen down-regulates ICAM-1 expression induced by hypoxia and hypoglycemia: the role of NOS. *Am J Physiol Cell Physiol.* 2000;278:C292–C302.
29. Weiland U, Haendeler J, Ihling C, et al. Inhibition of endogenous nitric oxide synthase potentiates ischemia-reperfusion-induced myocardial apoptosis via a caspase-3 dependent pathway. *Cardiovasc Res.* 2000;45:671–678.
30. Dorheim TA, Hoffman A, Van Wylen DG, et al. Enhanced interstitial fluid adenosine attenuates myocardial stunning. *Surgery.* 1991;110:136–145.
31. Babbitt DG, Virmani R, Vildibill HD Jr, et al. Intracoronary adenosine administration during reperfusion following 3 hours of ischemia: effects on infarct size, ventricular function, and regional myocardial blood flow. *Am Heart J.* 1990;120:808–818.
32. Norton ED, Jackson EK, Virmani R, et al. Effect of intravenous adenosine on myocardial reperfusion injury in a model with low myocardial collateral blood flow. *Am Heart J.* 1991;122:1283–1291.
33. Richardt G, Waas W, Kranzhofer R, et al. Adenosine inhibits exocytotic release of endogenous noradrenaline in rat heart: a protective mechanism in early myocardial ischemia. *Circ Res.* 1987;61:117–123.
34. Sato H, Hori M, Kitakaze M, et al. Endogenous adenosine blunts β -adrenoceptor-mediated inotropic response in hypoperfused canine myocardium. *Circulation.* 1992;85:1594–1603.
35. Cronstein BN, Levin RI, Belanoff J, et al. Adenosine: an endogenous inhibitor of neutrophil-mediated injury to endothelial cells. *J Clin Invest.* 1986;78:760–770.
36. Kitakaze M, Hori M, Sato H, et al. Endogenous adenosine inhibits platelet aggregation during myocardial ischemia. *Circ Res.* 1991;69:1402–1408.
37. Hausenloy DJ, Yellon DM. New directions for protecting the heart against ischaemia-reperfusion injury: targeting the reperfusion injury salvage kinase (RISK)-pathway. *Cardiovasc Res.* 2004;61:448–460.
38. Trincavelli ML, Tusciano D, Marroni M, et al. Involvement of mitogen protein kinase cascade in agonist-mediated human A_2 adenosine receptor regulation. *Biochim Biophys Acta.* 2002;1591:55–62.
39. Yang XM, Krieg T, Cui L, et al. NECA and bradykinin at reperfusion reduce infarction in rabbit hearts by signaling through PI3K, ERK, and NO. *J Mol Cell Cardiol.* 2004;36:411–421.
40. Boucher M, Pesant S, Falcao S, et al. Post-ischemic cardioprotection by A_2A adenosine receptors: dependent of phosphatidylinositol 3-kinase pathway. *J Cardiovasc Pharmacol.* 2004;43:416–422.
41. Kawasaki K, Smith RS Jr, Hsieh CM, et al. Activation of the phosphatidylinositol 3-kinase-protein kinase Akt pathway mediates nitric oxide-induced endothelial cell migration and angiogenesis. *Mol Cell Biol.* 2003;23:5726–5737.
42. Richardt G, Waas W, Kranzhofer R, et al. Interaction between the release of adenosine and noradrenaline during sympathetic stimulation: a feed-back mechanism in rat heart. *J Mol Cell Cardiol.* 1989;21:269–277.
43. Buga GM, Griscavage JM, Rogers NE, et al. Negative feedback regulation of endothelial cell function by nitric oxide. *Circ Res.* 1993;73:808–812.